

FUNDAMENTAL APPROACH TO ESTIMATING THE ACTUAL CHARGE OF A PARTIAL DISCHARGE IN A GIS USING A THREE-DIMENSIONAL ELECTROMAGNETIC ANALYSIS

T. Hoshino^{1*}, S. Maruyama¹ and T. Nakajima¹

¹Toshiba Corporation, 2-1, Ukishima-cho, Kawasaki, Japan

*Email: <toshihiro.hoshino@toshiba.co.jp>

Abstract: For the first time, using the Finite-difference time-domain (FDTD) method, the actual charge has been quantitatively combined with experimental electromagnetic waves detected by PD-detecting couplers without an apparent charge. In the case of a metallic particle bouncing on the inner surface of the enclosure, the FDTD analysis is sufficient to simulate the practical propagation of electromagnetic waves due to partial discharge (PD) from the aspects of both voltage output and cumulative energy.

1 INTRODUCTION

We have introduced a three-dimensional electromagnetic analysis using the Finite-difference time-domain (FDTD) method to analyze the propagation of electromagnetic waves attenuating through insulation materials and T-branches in a gas-insulated switchgear (GIS). The analysis helps us to design a PD-detecting coupler with appropriate sensitivity and arrange couplers at appropriate locations in a GIS. The most important issue regarding the analysis is to enable calibration of the actual charge of a partial discharge (PD) from the output of a PD-detecting coupler using the analytical sensitivity correlation, which is the relationship between the actual charge and the output of the PD-detecting coupler.

We have clarified that electromagnetic waves are advantageous for accurately estimating the actual charge rather than the displacement current that leads to an apparent charge according to IEC 60270 [1]. However, a previous paper [2] only shows attenuation ratios whose values are derived from the peak-to-peak value of an electric field (V/m_{p-p}). The peak-to-peak value depends strongly on reflections of electromagnetic waves. Besides, the dimension of the electric field values (V/m) is different from that of the actual charge (pC) and the voltage output (V) of the PD-detecting coupler, which makes it difficult to obtain an analytical sensitivity correlation. Therefore, we use the radius integral of the electric fields inside a coaxial cable to obtain the voltage output of the PD-detecting coupler. The cumulative energy calculated from the voltage output is also introduced to double-check attenuation characteristics through insulation materials.

2 ANALYTICAL CONDITIONS

Figure 1 (a) shows the analytical model simulating electromagnetic waves due to PD propagating inside a GIS bus bar, which is the same as the experimental setup. A Gaussian pulse and the

corresponding voltage outputs of the PD-detecting coupler (Disc 0) $v_{Disc 0}$ are also shown in Fig. 1. A previous paper [2] explained in detail such analytical issues as modeling, cell splitting, and pulse injection; therefore, this paper describes only those issues that have been improved since the previous paper [2] was submitted.

Three types of metallic particle are considered as PD sources, as shown in Fig. 1 (b). A Gaussian pulse with both a rise time of 240 (ps) and a fall time of 240 (ps) shown in Fig. 1 (c) was injected at the same locations where the three types of particle were individually fixed in the experiment. Because a Gaussian pulse whose dimension is Ampere (A) can be designated directly instead of an electric field (V/m) in the upgraded FDTD software, we can calculate the corresponding magnitude (pC) of the Gaussian pulse as shown in Fig. 1 (c). The magnitude of the Gaussian pulse is adjusted to 10 (pC) according to the following equation.

$$q = \int i(t) \cdot dt \quad \dots\dots\dots (1)$$

Although it is very difficult to measure the actual PD pulse directly in a practical GIS bus bar, fundamental research clarifies a reliable PD pulse waveform [3]. Therefore, an appropriate Gaussian pulse has been selected for our analysis.

Figure 2 shows method of calculating the voltage output v_{Disc} (mV_{p-p}) within a coaxial cable having an inner diameter of ϕ 3.0 (mm) and an outer diameter of ϕ 12.0 (mm). By dividing each peak-to-peak value of $v_{Disc A}$, $v_{Disc B}$, $v_{Disc C}$ by another value of $v_{Disc 0}$, each transmissivity T_v can be obtained as shown in Eq. (2).

$$T_v = \left\{ \frac{v_{Disc A}}{v_{Disc 0}}, \frac{v_{Disc B}}{v_{Disc 0}}, \frac{v_{Disc C}}{v_{Disc 0}} \right\} \dots\dots\dots (2)$$

T_v consists of three values and signifies the transmissivity of electromagnetic waves due to PD

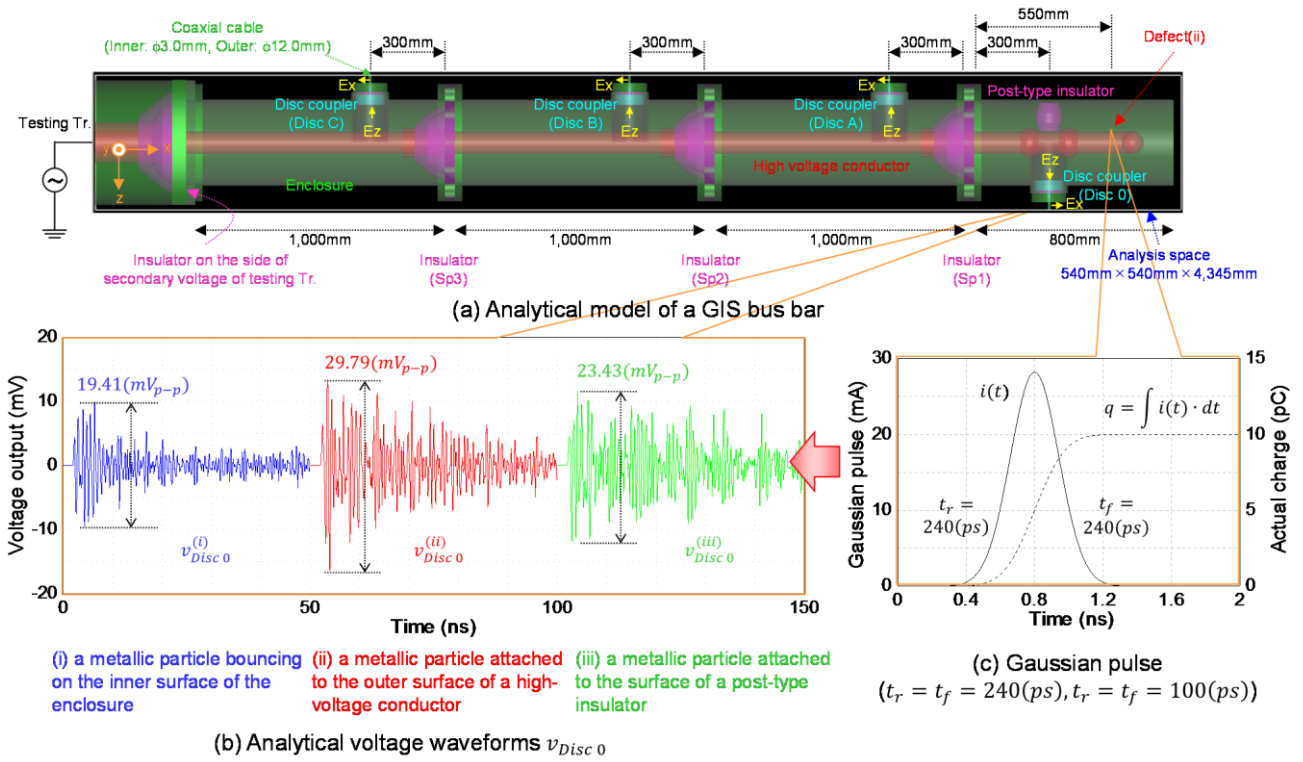


Figure 1: Analytical conditions for analyzing electromagnetic waves due to PD propagating inside a GIS bus bar

attenuating through insulation materials, from the aspect of v_{Disc} . However, E_{x1} shown in Fig. 2, instead of v_{Disc} , was applied to the calculation of T_E in the previous paper [1]-[2], that is,

$$T_E = \left\{ \frac{E_{x1\ Disc\ A}}{E_{x1\ Disc\ 0}}, \frac{E_{x1\ Disc\ B}}{E_{x1\ Disc\ 0}}, \frac{E_{x1\ Disc\ C}}{E_{x1\ Disc\ 0}} \right\} \dots\dots (3)$$

In contrast, in this paper, the voltage output v_{Disc} of all PD couplers regarding all types of defect can be calculated by integrating the electric field E_x as shown in Fig. 2 and Eq. (4), after solving $\{E_x, E_y, E_z\}$ of the whole cells using the FDTD analysis.

$$v_{Disc} = - \int_{x_q}^{x_p} E_x \cdot dx = \sum_{i=1}^5 E_{xn} \cdot \Delta x_n \dots\dots\dots (4)$$

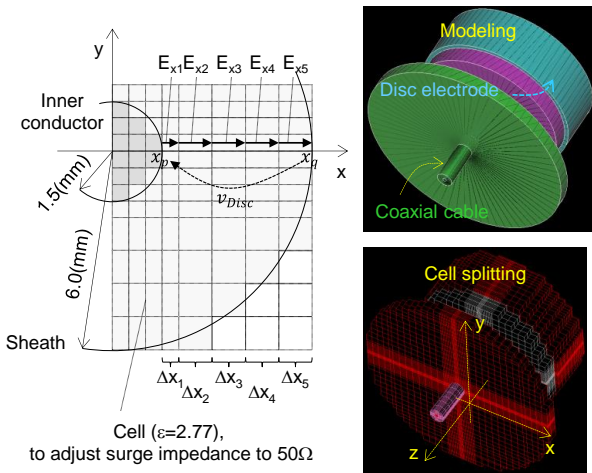


Figure 2: Method of calculating voltage output v_{Disc} within a coaxial cable

Consequently, using Eqs. (1) and (4), the voltage output of the PD-detecting coupler v_{Disc} (mV_{p-p}) can be combined with the actual charge q (pC).

3 DIRECT COMPARISON OF VOLTAGE OUTPUT BETWEEN EXPERIMENT AND FDTD ANALYSIS

Figure 1 (b) shows analytical voltage outputs $v_{Disc}^{(i)}$, $v_{Disc}^{(ii)}$, $v_{Disc}^{(iii)}$ that correspond to the same actual charge of 10 (pC), by using the radial integral of the electric field E_x obtained by the FDTD analysis. For the first time, the actual charge q is quantitatively combined with the voltage output of the PD-detecting coupler v_{Disc} as shown in Eq. (5).

$$q = 10(pC) \leftrightarrow v_{Disc}^{(i)} = 19.41(mV_{p-p}) \dots\dots\dots (5)$$

The difference in voltage outputs of defects, which is defined as the ratio of $v^{(any)}$ to $v^{(ii)}$, is also shown below,

$$\frac{v_{Disc}^{(ii)}}{v_{Disc}^{(ii)}} = 100(\%) > \frac{v_{Disc}^{(iii)}}{v_{Disc}^{(ii)}} = 78.66(\%) > \frac{v_{Disc}^{(i)}}{v_{Disc}^{(ii)}} = 65.16(\%) \dots\dots\dots (6)$$

It is considered from Eq. (6) that the output ratios are not so different for the various defects (i) – (iii) if the actual charge has the same magnitude.

The output ratios for defects obtained by the experiment [4], however, differ from Eq. (6)

obtained by the FDTD analysis. For example, in the case of a 420 kV-class testing bus bar, the output ratio regarding a defect is $\frac{v_{Disc}^{(i)}}{v_{Disc}^{(ii)}} = 2500(\%)$ when the apparent charge is 10 (pC) [4]. As for defect (i), the apparent charge obtained by the experiment might be underestimated [1] compared to the actual charge obtained by the analytical sensitivity correlation shown in Eq. (5). It is speculated that the apparent charge is not proportional to the actual charge under conditions where a large coaxial cylinder such as a GIS is connected directly to a PD-detecting instrument complying with IEC 60270. Therefore, particularly in the case of diagnosing a GIS, electromagnetic waves are advantageous for accurately estimating the actual charge rather than the displacement current that leads to the apparent charge.

Figure 3 shows the attenuation characteristics of v_{Disc} through insulation materials under $q = 10(pC)$. The solid lines are obtained in the case of a Gaussian pulse with $t_r = t_f = 240(ps)$ while the broken lines are obtained in the case of $t_r = t_f = 100(ps)$. The faster t_r, t_f increases the voltage outputs v_{Disc} under any defect conditions. The $v_{Disc A}, v_{Disc B}, v_{Disc C}$ attenuated through a few insulation materials are half or one third as many as the $v_{Disc 0}$. Although the output ratio for defects and the transmissivity T_v can be changed depending on t_r, t_f , there is no possibility of $\frac{v_{Disc}^{(i)}}{v_{Disc}^{(ii)}} = 2500(\%)$ being obtained from the experiment based on an apparent charge.

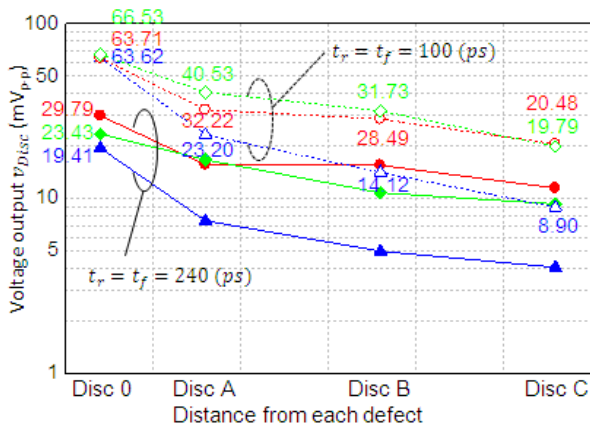
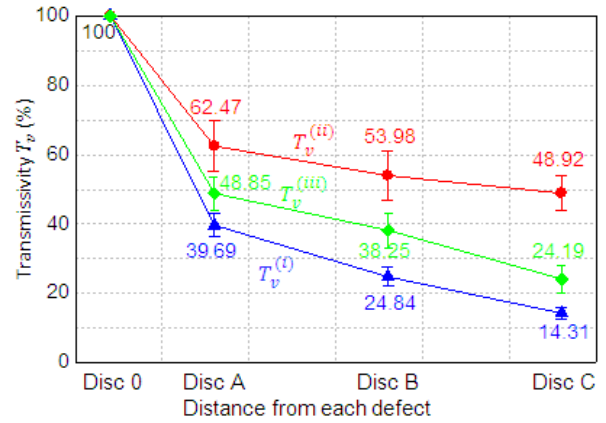


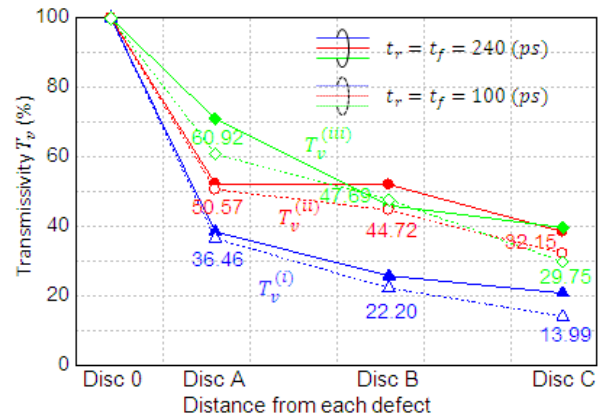
Figure 3: Attenuation characteristics of v_{Disc} through insulation materials under $q = 10(pC)$

Figure 4 shows a comparison of transmissivities T_v between experiment and FDTD analysis. Figure 4 (a) is obtained from the experiment and Fig. 4 (b) is based on Fig. 3, which is derived from the FDTD analysis. Both experiment and FDTD analysis correspond well for $T_v^{(i)}$, particularly in the case of $t_r = t_f = 100(ps)$. Meanwhile, the correspondence of the transmissivity is not quite the same as $T_v^{(ii)}$

and $T_v^{(iii)}$. Although T_v plays the significant role of ensuring the accuracy of the FDTD analysis, only T_v has its own limits for identifying t_r, t_f of a Gaussian pulse.



(a) T_v from the experiment



(b) T_v from the FDTD analysis

Figure 4: Comparison of transmissivity T_v between experiment and FDTD analysis

4 DIRECT COMPARISON OF CUMULATIVE ENERGY BETWEEN EXPERIMENT AND FDTD ANALYSIS

Figure 5 is a flowchart of the cumulative energy W_{Disc} calculated from the voltage output of PD-detecting coupler v_{Disc} . Figure 5 shows an example of v_{Disc} acquired using an oscilloscope with a digital sampling rate of 10 (GS/s), and also shows the time integral of v_{Disc} with and without noise reduction. The simple time integral is defined as Eq. (7).

$$\frac{1}{R} \cdot \sum_{k=1}^n v_{Disc}(k)^2 \cdot \Delta t \quad \dots \dots (7)$$

The surge impedance of a coaxial cable is $R=50(\Omega)$, and the digital sampling rate of 10 (GS/s)

automatically represents $\Delta t = 100(ps)$. White noise detected with the oscilloscope is accumulated using only a simple time integral. The appropriate cumulative energy $W_{Disc}(n)$ can be obtained using Eq. (8), shown in Fig. 5, by eliminating cumulative noise C_{noise} given as Eq. (9) from the simple time integral shown in Eq. (7).

$$W_{Disc}(n) = \frac{1}{R} \cdot \sum_{k=1}^n v_{Disc}(k)^2 \cdot \Delta t - n \cdot C_{noise} \quad \dots (8)$$

$$C_{noise} = \frac{1}{R} \cdot \frac{\sum_{k=1}^{n_2} v_{Disc}(k)^2 \cdot \Delta t - \sum_{k=1}^{n_1} v_{Disc}(k)^2 \cdot \Delta t}{n_2 - n_1} \quad \dots (9)$$

n_1 and n_2 are arbitrary times when PD signals do not occur, and, for example, $n_1=10000$ and $n_2=20000$ are selected in Fig. 5. Equations (8) and (9) are applied only to experimental waveforms, because the analytical ones shown in Fig. 1 (c) have no cumulative noise C_{noise} .

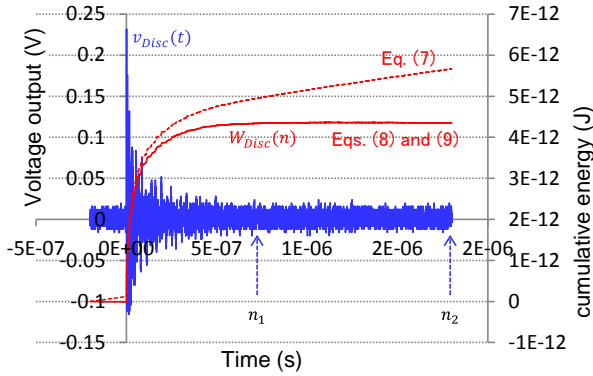


Figure 5: Flowchart for calculating cumulative energy W_{Disc} from voltage output v_{Disc}

Tables 1 and 2 show the cumulative energy W_{Disc} and the corresponding transmissivity T_W in the cases of $t_r = t_f = 240(ps)$ and $t_r = t_f = 100(ps)$, respectively. Figure 6 shows the attenuation characteristics of the cumulative energy W_{Disc} based on Tables 1 and 2. It is obvious as shown in Fig. 6 that cumulative energy under the condition of $t_r = t_f = 100(ps)$ is about six to ten times that under the condition of $t_r = t_f = 240(ps)$ even if the actual charge is the same value of 10 (pC).

Figure 7 shows transmissivity T_W based on cumulative energy W_{Disc} shown in Tables 1 and 2. Each T_W can be obtained as shown below,

$$T_W = \left\{ \frac{W_{Disc A}}{W_{Disc 0}}, \frac{W_{Disc B}}{W_{Disc 0}}, \frac{W_{Disc C}}{W_{Disc 0}} \right\} \dots \dots \dots (10)$$

Table 1: Cumulative energy W_{Disc} and transmissivity T_W in the case of $t_r = t_f = 240(ps)$

Defect	Disc 0	Disc A	Disc B	Disc C
$W_{Disc}^{(i)}$	$5.21 \cdot 10^{-15}$	$1.78 \cdot 10^{-15}$	$1.03 \cdot 10^{-15}$	$4.40 \cdot 10^{-16}$
$T_W^{(i)}$	100%	34.2%	19.7%	8.44%
$W_{Disc}^{(ii)}$	$1.55 \cdot 10^{-14}$	$6.39 \cdot 10^{-15}$	$4.73 \cdot 10^{-15}$	$2.66 \cdot 10^{-15}$
$T_W^{(ii)}$	100%	41.2%	30.5%	17.1%
$W_{Disc}^{(iii)}$	$1.50 \cdot 10^{-14}$	$8.15 \cdot 10^{-15}$	$2.96 \cdot 10^{-15}$	$2.07 \cdot 10^{-15}$
$T_W^{(iii)}$	100%	54.2%	19.7%	13.8%

Table 2: Cumulative energy W_{Disc} and transmissivity T_W in the case of $t_r = t_f = 100(ps)$

Defect	Disc 0	Disc A	Disc B	Disc C
$W_{Disc}^{(i)}$	$5.38 \cdot 10^{-14}$	$1.19 \cdot 10^{-14}$	$6.48 \cdot 10^{-15}$	$2.19 \cdot 10^{-15}$
$T_W^{(i)}$	100%	22.1%	12.0%	4.07%
$W_{Disc}^{(ii)}$	$9.87 \cdot 10^{-14}$	$2.95 \cdot 10^{-14}$	$1.69 \cdot 10^{-14}$	$8.68 \cdot 10^{-15}$
$T_W^{(ii)}$	100%	29.9%	17.2%	8.79%
$W_{Disc}^{(iii)}$	$1.09 \cdot 10^{-13}$	$4.41 \cdot 10^{-14}$	$1.93 \cdot 10^{-14}$	$9.53 \cdot 10^{-15}$
$T_W^{(iii)}$	100%	40.4%	17.7%	8.73%

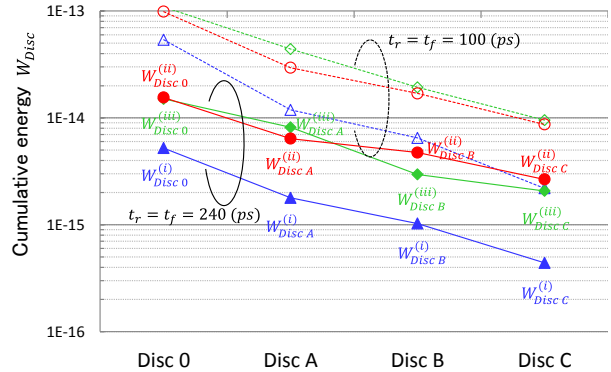


Figure 6: Attenuation characteristics of W_{Disc} obtained by FDTD analysis

It is obvious as shown in Fig. 7 that T_W under the condition of $t_r = t_f = 100(ps)$ tends to decrease rapidly compared to T_W under the condition of $t_r = t_f = 240(ps)$. Therefore, a faster t_r, t_f means larger cumulative energy (Fig. 6) and rapid attenuation (Fig. 7).

Figure 8 shows transmissivity T_W based on cumulative energy W_{Disc} in the cases of the experiment. By comparing the FDTD analysis shown in Fig. 7 with the experiment shown in Fig. 8, $T_W^{(i)}$ is in good correspondence in the case of $t_r = t_f = 100(ps)$. Therefore, it is obvious from the aspects of both $T_v^{(i)}$ and $T_W^{(i)}$ that the FDTD analysis is sufficient to simulate the practical propagation of the electromagnetic waves due to PD, as to (i) a metallic particle bouncing on the

inner surface of the enclosure. However, there are many differences in $T_W^{(ii)}$ between the experiment and the FDTD analysis while $T_v^{(ii)}$ mentioned previously is not so different as shown in Fig. 4. The reasons why $T_W^{(ii)}$ is different are unknown so far, but, firstly, travelling energy consisting of lower frequency components is easily reflected at a testing transformer shown in Fig. 1 (a); therefore, PD-detecting couplers might detect both travelling and reflecting energies. Secondly, the PD pulse waveform might not be a Gaussian pulse.

As for (iii), a metallic particle attached to the surface of a post-type insulator, measured $v_{Disc}^{(iii)}$ is very small, which makes the precision of signal processing shown in Fig. 5 low. Further improvements regarding both the experiment and FDTD analysis are required under the conditions of (ii) and (iii).

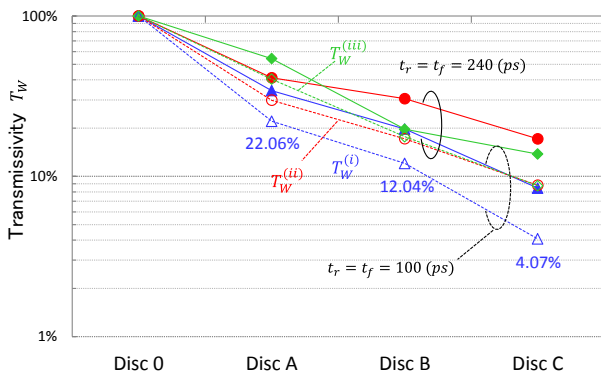


Figure 7: Transmissivity T_W based on cumulative energy W_{Disc} obtained by FDTD analysis

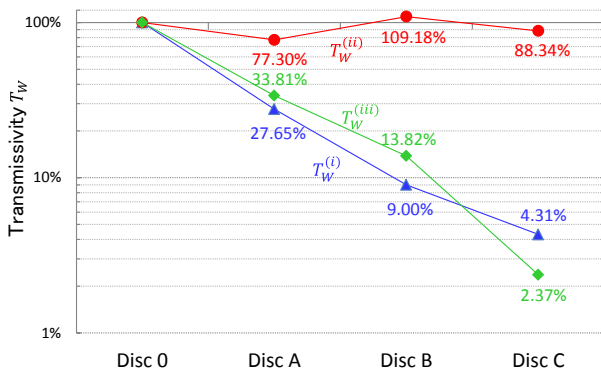


Figure 8: Transmissivity T_W based on cumulative energy W_{Disc} obtained by experiment

5 PROCESS OF ESTIMATING ACTUAL CHARGE FROM EXPERIMENTAL OUTPUT OF PD-DETECTING COUPLER

The estimation of the actual charge from the experimental outputs is discussed quantitatively using both voltage output and cumulative energy. Because the results for (ii) and (iii) are still not reliable, the fundamental approach to estimating

the actual charge is applied only to defect (i) in this section. In the case of $t_r = t_f = 100(ps)$, the analytical sensitivity correlation between the actual charge q and the voltage output $v_{Disc0}^{(i)}$ of the PD-detecting coupler (Disc 0) can be shown as Eq. (5') based on Fig. 3.

$$q = 10(pC) \leftrightarrow v_{Disc0}^{(i)} = 63.62(mV_{p-p}) \dots \dots \dots (5')$$

Because the actual charge is proportional to v_{Disc} , the following equation can be obtained.

$$10^{-11}(C):v_{Disc}(mV_{p-p}) = y(C):x(mV_{p-p}) \dots \dots (11)$$

By substituting Eq. (5') into v_{Disc} of Eq. (11), each actual charge $y(C)$ that corresponds to the experimental voltage output $x(mV_{p-p})$ can be calculated. The process is available under any defect conditions if the accuracy of the above sensitivity correlation such as Eq. (5') is guaranteed.

The actual charge can also be analytically combined with the cumulative energy of the PD-detecting coupler W_{Disc} as shown in Tables 1 and 2. For example, in the case of $t_r = t_f = 100(ps)$,

$$q = 10(pC) \leftrightarrow W_{Disc0}^{(i)} = 5.3846 \cdot 10^{-14}(J) \dots (12)$$

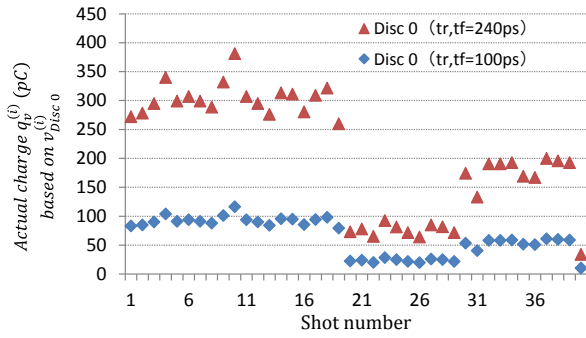
Because the square of the actual charge is proportional to W_{Disc} , the following equation can be obtained.

$$\{10^{-11}(C)\}^2:W_{Disc}(J) = \{y(C)\}^2:x(J) \dots \dots \dots (13)$$

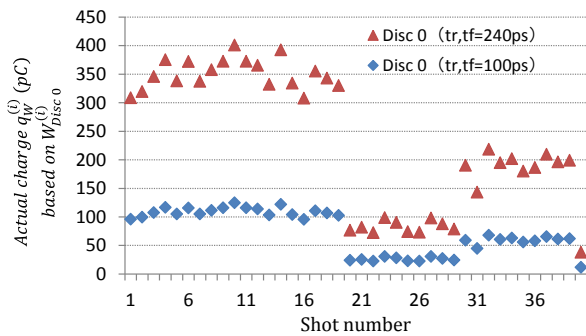
By substituting Eq. (12) into W_{Disc} of Eq. (13), each actual charge $y(C)$ that corresponds to the experimental cumulative energy $x(J)$ can be calculated.

Figure 9 shows the estimated actual charges $q_v^{(i)}, q_W^{(i)}$ from applying Eqs. (11) and (13) to the experimental outputs of PD-detecting coupler (Disc 0) that are obtained under the condition of defect (i). The horizontal axis indicates shot numbers. Because it has already been clarified in the previous section that the FDTD analysis is sufficient to simulate the practical propagation of electromagnetic waves for defect (i) in the case of $t_r = t_f = 100(ps)$, \blacklozenge -marks in Fig. 9 show reliable values as $q_v^{(i)}, q_W^{(i)}$. Figure 9 indicates that when a metallic particle with a 10-millimeter length bounds on the bare surface of the GIS bus bar the magnitude of PD becomes several tens of pC or about 100 (pC). These estimated values of the actual charge differ from the measured values of an apparent charge whose magnitudes are up to 10 (pC). It is obvious as shown in Figs. 9 that the choice of slower t_r, t_f represented by \blacktriangle -marks

causes an overvalued actual charge, which indicates that the selection of t_r, t_f is the key to the calibration.



(a) Actual charge $q_v^{(i)}$ based on $v_{Disc0}^{(i)}$



(b) Actual charge $q_W^{(i)}$ based on $W_{Disc0}^{(i)}$

Figure 9: Estimated actual charges $q_v^{(i)}, q_W^{(i)}$ from the experimental outputs of PD-detecting coupler (Disc 0)

Figure 10 shows the correlation of the actual charges between $q_v^{(i)}$ and $q_W^{(i)}$. Because both $v_{Disc0}^{(i)}$ and $W_{Disc0}^{(i)}$ of the same shot number are derived from the same experimental waveform, the actual charge of the same shot number has to be $q_v^{(i)} = q_W^{(i)}$. Although the tendency of $q_W^{(i)} > q_v^{(i)}$ is observed slightly, there is a good correlation between both $q_v^{(i)}$ and $q_W^{(i)}$. Figure 10 clarifies that both $v_{Disc0}^{(i)}$ and $W_{Disc0}^{(i)}$ are available for estimating the actual charge under any defect conditions if the accuracy of the sensitivity correlation such as Eq. (5') is guaranteed.

The sensitivity correlation can vary with a number of factors, such as PD pulse shape with various t_r, t_f and amplitude, attenuation through insulation materials and T-branches, and frequency dispersion regarding electromagnetic waves of high-order modes. The FDTD analysis takes into account all of the circumstances in principle, assuming that cell splitting is very small. Therefore, the sensitivity correlation is a fully-considered solution without any leaps of logic.

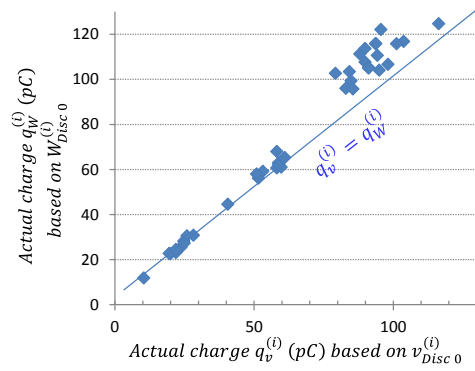


Figure 10: Correlation of actual charges between $q_v^{(i)}$ and $q_W^{(i)}$

6 CONCLUSION

For the first time, an actual charge has been quantitatively combined with experimental electromagnetic waves detected by PD-detecting couplers without an apparent charge. In the case of a metallic particle bouncing on the inner surface of the enclosure, the FDTD analysis is sufficient to simulate the practical propagation of electromagnetic waves due to PD from the aspects of both voltage output and cumulative energy.

7 REFERENCES

- [1] T. Hoshino, S. Maruyama and T. Sakakibara, "New Approach to Calibration of PD Magnitude Regarding GIS Using Three-Dimensional Electromagnetic Analysis," in Proc. of the CMD2010, vol. 2, No. P1-56, pp. 866-869, Sep. 2010.
- [2] T. Hoshino, S. Maruyama and T. Sakakibara, "Simulation of Propagating Electromagnetic Wave due to Partial Discharge in GIS using FDTD," IEEE Trans. Power Delivery, vol. 24, No. 1, pp. 153-159, Jan. 2009.
- [3] M. D. Judd, L. Yang and I. J. Craddock, "Locating Partial Discharges using UHF Measurements: A Study of Signal Propagation using the Finite-Difference Time-Domain Method," in Proc. of the 14th ISH, G-019, 2005.
- [4] T. Hoshino, H. Koyama, S. Maruyama and M. Hanai, "Comparison of Sensitivity between UHF Method and IEC 60270 for On-site Calibration in Various GIS," IEEE Trans. Power Delivery, vol. 21, No. 4, pp. 1948-1953, Oct. 2006.